Gadofosveset-Based Biomarker of Tissue Albumin Concentration: Technical Validation In Vitro and Feasibility In Vivo

Owen C. Richardson,[1] Octavia Bane,[2] Marietta L.J. Scott,[3] Steven F. Tanner,[4] John C. Waterton,[3] Steven P. Sourbron,[1] Timothy J. Carroll,[2] and David L. Buckley[1]*

Purpose: There is currently no adequate method of mapping physiologic and pathophysiologic tissue albumin concentrations in human subjects. The objective of this study was to devise and evaluate a biomarker of regional albumin concentration using gadofosveset-enhanced MRI.
Theory and Methods: A binding and relaxation model was devised and evaluated in vitro in solutions of albumin at 3.0 Tesla (T) and 4.7T. The method was evaluated in the heart in seven volunteers at 3.0T.
Results: MRI-derived estimates of albumin concentration were in good agreement with true values over the range 0.1–1.0 mM (Pearson correlation coefficients of 0.85 and 0.88 for 3.0T and 4.7T, respectively). The mean calculated albumin concentration in the myocardium for the volunteers was 0.02 mM (range, 0.01–0.03 mM).
Conclusion: Accurate estimates of albumin concentration in vitro suggest this may be a viable noninvasive alternative to existing techniques. In the myocardium the MRI-derived estimates of albumin concentration indicate the practical feasibility of the technique but were below expected values. Gadofosveset-enhanced MR relaxometry has potential in providing biomarkers of regional albumin concentration; further evaluation is required before it can be used reliably in vivo. **Magn Reson Med 73:244–253, 2015. © 2014 University of Leeds. Magnetic Resonance in Medicine published by Wiley Periodicals, Inc. This is an open access article under the terms of the Creative Commons Attribution License, which permits use, distribution and reproduction in any medium, provided the original work is properly cited.**

Key words: gadofosveset; albumin; biomarker; binding; relaxivity

[1]Division of Medical Physics, University of Leeds, Leeds, United Kingdom.
[2]Departments of Biomedical Engineering and Radiology, Northwestern University, Chicago, Illinois, USA.
[3]Personalized Healthcare and Biomarkers, AstraZeneca, Macclesfield, Cheshire, United Kingdom.
[4]Department of Medical Physics and Engineering, Leeds Teaching Hospitals NHS Trust, Leeds, United Kingdom.
*Correspondence to: David L. Buckley, Ph.D., Division of Medical Physics, University of Leeds, Room 8.001, Worsley Building, Clarendon Way, Leeds, LS2 9JT UK. E-mail: d.l.buckley@leeds.ac.uk

INTRODUCTION

Albumin is the most abundant protein in human plasma, accounting for half of all serum proteins (1). It transports, by means of its numerous binding sites, endogenous compounds (2) and drugs (3), and is essential in regulating the flow of water between blood and tissue (1). Around 33% of albumin in the body is intravascular, with 49% in exchangeable extravascular locations and the remainder in remote extravascular compartments such as the skin (4). An imbalance in intra–extravascular albumin may potentially result in edema. Albumin concentrations may be accurately measured in urine or blood samples, with altered levels caused by changes in rates of synthesis, catabolism or extravascular leakage. Low levels of albumin have been linked to critical illness (5) and may be a risk factor for myocardial infarction (6). The body's natural transcapillary exchange rate of around 5% of intravascular albumin per hour (7) may increase in damaged or angiogenic vessels. Localized increases in extravascular macromolecular content may be symptomatic of, for example, reperfused myocardial infarction (8) or tumor angiogenesis (9).

Although albumin concentrations in blood and urine are valuable indicators of albumin imbalance, they do not fully describe its biodistribution. Direct measurement of interstitial albumin concentration is not straightforward, with varying results found using invasive techniques such as wick implantation (10), blister suction (11) or double lumen catheterization (12). It is suggested that a noninvasive biomarker (13) of localized extravascular albumin may facilitate quantitative assessment of extravascular leakage. This may have prognostic and/or diagnostic value in assessment of tumor angiogenesis or myocardial infarction, for example, and may also be used for prospective assessment of response to treatment. Although conventional small-molecule gadolinium (Gd) contrast agents are frequently used in MRI to assess microvascular permeability, macromolecular Gd agents have shown increased sensitivity to malignancy (14), response to anti-angiogenic treatment (15) and ischemic microvascular damage (16).

Gadofosveset trisodium (Ablavar, Lantheus Medical Imaging, N Billerica, MA, previously marketed as Vasovist, Schering AG, Germany) is a Gd-containing contrast agent, with a stable gadopentetate core and phosphodiester linkage to a lipophilic albumin-binding group (17). In humans, over 90% of injected gadofosveset is reported to bind reversibly to serum albumin (18), increasing the effective molecular weight of the contrast agent from 957 Da to 68 kDa (19). Binding alters the pharmacokinetics of the molecule, reducing its extravasation and excretion rates; consequently the agent is well suited to angiography

(20). Beyond angiography, recent studies have utilized gadofosveset in assessment of human brain tumors (21), liver lesions (22), chronic myocardial infarction (23), atherosclerosis (24), and liver fibrosis (25), and in combination with spin locking in vitro (26).

Substantially higher longitudinal and transverse relaxivities are observed for gadofosveset at low magnetic field strengths upon binding (27), due to the lower tumbling rate and longer correlation time of the bound molecule (28). The longitudinal and transverse relaxivities of the free (unbound) molecule are slightly higher than those of a conventional (nonbinding) small-molecule Gd-based agent such as gadopentetate (29). At physiologically applicable concentrations, it may be assumed that one gadofosveset molecule binds to a single albumin molecule (18,30). In this case, the bound fraction of gadofosveset is at a maximum where albumin exceeds gadofosveset concentration and declines where gadofosveset exceeds albumin concentration. This relationship suggests that, under certain conditions, it may be possible to use gadofosveset binding fraction as a biomarker for albumin concentration. However, signal intensity changes induced by the bound and free gadofosveset molecules cannot be directly separated in vivo and therefore binding fraction must be acquired through mathematical modeling.

This study aims to assess the viability of utilizing measured gadofosveset-enhanced longitudinal (R_1, $1/T_1$) and transverse (R_2, $1/T_2$) relaxation rates to develop a biomarker of albumin concentration in vitro. This method could be applied to generate a spatially located measure of tissue albumin which could be used as an alternative to current invasive techniques. Model feasibility is assessed using R_1 and R_2 measurements in vitro and in left ventricular blood and myocardial tissue of healthy human volunteers at 3.0 Tesla (T). Identification of abnormal extravascular albumin distribution correlating to increased capillary leakage may have several applications, including early indication of disease progression or treatment response in tumor angiogenesis, or assessment of reperfused myocardial infarction.

THEORY

Measuring Albumin Binding Fraction

For conventional Gd-based contrast agents, a single longitudinal relaxivity (r_1) is usually sufficient to describe the relationship between the contrast-agent induced change in R_1 (ΔR_1) and gadofosveset concentration (C_g); likewise a single transverse relaxivity (r_2) describes the relationship between ΔR_2 and C_g:

$$\Delta R_i = r_i . C_g \qquad [1]$$

where $i = 1,2$.

For albumin-binding gadofosveset, composite relaxivities are observed, comprising contributions from both the bound and free molecule. For the B_0 field strengths used in this study, relaxivity of the bound molecule exceeds that of the free molecule. For the free molecule, the relationship in Eq. [1] may be assumed. For the bound molecule, there is a nonlinear relationship between C_g and $R_{1,2}$ (although at high field r_{1bound} approaches r_{1free} and the relationship

between C_g and R_1 tends to linearity). The overall gadofosveset and serum albumin (C_{sa}) concentrations may be defined as the sum of their bound and free components:

$$C_g = C_{gbound} + C_{gfree} \qquad [2]$$

$$C_{sa} = C_{sabound} + C_{safree} \qquad [3]$$

At low B_0 field strengths, the distinct relaxivities of the bound and free gadofosveset molecules must be considered:

$$\Delta R_1 = r_{1bound} . C_{gbound} + r_{1free} . C_{gfree} \qquad [4]$$

$$\Delta R_2 = r_{2bound} . C_{gbound} + r_{2free} . C_{gfree} \qquad [5]$$

Assuming ΔR_1 and ΔR_2 can be measured and r_{1bound}, r_{1free}, r_{2bound}, and r_{2free} are known, it is possible to rearrange Eqs. [4] and [5] to give expressions for bound and free gadofosveset concentration:

$$C_{gbound} = \frac{r_{2free} . \Delta R_1 - r_{1free} . \Delta R_2}{r_{1bound} . r_{2free} - r_{2bound} . r_{1free}} \qquad [6]$$

$$C_{gfree} = \frac{r_{1bound} . \Delta R_2 - r_{2bound} . \Delta R_1}{r_{1bound} . r_{2free} - r_{2bound} . r_{1free}} \qquad [7]$$

Combining Eqs. [6] and [7] according to Eq. [2] gives:

$$C_g = \frac{\Delta R_2 (r_{1bound} - r_{1free}) - \Delta R_1 (r_{2bound} - r_{2free})}{r_{1bound} . r_{2free} - r_{1free} . r_{2bound}} \qquad [8]$$

Bound, free, and overall gadofosveset concentrations can therefore be derived from measurement of ΔR_1 and ΔR_2.

Measuring Albumin Concentration

In a second step, gadofosveset concentration is related to albumin concentration by assuming a chemical equilibrium between free and bound substances. The noncovalent binding equilibrium between a paramagnetic substrate and a protein is defined as (31):

$$[Substrate] + [Protein] \rightleftharpoons [Substrate–Protein]$$
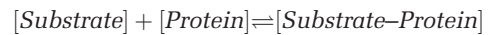
The association constant, or binding affinity (K_a), involving a single equivalent binding site may be expressed as (31):

$$K_a = \frac{[Substrate–Protein]}{[Substrate] . [Protein]} .$$

Expressing this binding affinity in terms of gadofosveset and albumin concentrations:

$$K_a = \frac{C_{gbound}}{C_{gfree} . C_{safree}} \qquad [9]$$

Assuming a single bound gadofosveset molecule per serum albumin molecule:

$$C_{gbound} = C_{sabound} \qquad [10]$$

Eq. [9] becomes:

$$K_a = \frac{C_{\text{gbound}}}{C_{\text{gfree}} \cdot (C_{sa} - C_{\text{gbound}})}. \qquad [11]$$

Rearranging for C_{sa}:

$$C_{sa} = C_{\text{gbound}} + \frac{1}{K_a} \cdot \frac{C_{\text{gbound}}}{C_{\text{gfree}}} \qquad [12]$$

Inserting Eqs. [6] and [7] into Eq. [12] gives:

$$C_{sa} = \frac{r_{2\text{free}} \cdot \Delta R_1 - r_{1\text{free}} \cdot \Delta R_2}{r_{1\text{bound}} \cdot r_{2\text{free}} - r_{2\text{bound}} \cdot r_{1\text{free}}}$$
$$+ \frac{1}{K_a} \cdot \frac{r_{2\text{free}} \cdot \Delta R_1 - r_{1\text{free}} \cdot \Delta R_2}{r_{1\text{bound}} \cdot \Delta R_2 - r_{2\text{bound}} \cdot \Delta R_1}. \qquad [13]$$

Eq. [13], therefore, provides a method for deriving albumin concentration through measurement of ΔR_1 and ΔR_2, assuming fixed relaxivity and binding affinity values.

Measuring Bound Relaxivity

It remains to derive a method for measuring the relaxivity values from in vitro samples with known gadofosveset concentrations. Free relaxivity is derived using Eq. [1], applied to a solution without albumin. To derive a formula for bound relaxivity, C_{gfree} is first eliminated from Eq. [11] using Eq. [2], and the quadratic equation solved for C_{gbound}. Inserting the result into Eq. [4] or Eq. [5] gives an expression for ΔR_1 or ΔR_2 where only bound relaxivity is unknown:

$$\Delta R_i = r_{i\text{free}} \cdot C_g + (r_{i\text{bound}} - r_{i\text{free}}).$$
$$\left\{ \frac{(C_{sa} \cdot K_a + C_g \cdot K_a + 1) - \sqrt{\left[(C_{sa} \cdot K_a + C_g \cdot K_a + 1)^2 - 4 \cdot K_a^2 \cdot C_{sa} \cdot C_g \right]}}{2 \cdot K_a} \right\}$$
$$[14]$$

where $i = 1, 2$.

Only the negative form of the quadratic solution is applicable as the positive form would give a nonzero solution for C_{gbound} at $C_g = 0$. Eq. [14] has been represented in a similar form in several papers (for example, (30,32,33)). The model describes a gradual transition of binding fraction, from a maximum at low C_g, where observed relaxivity is dominated by $r_{1,2\text{bound}}$, toward a minimum at high C_g, where $r_{1,2\text{free}}$ has the greater influence (Fig. 1). As the model assumes a single binding site, the shift in emphasis from $r_{1,2\text{bound}}$ to $r_{1,2\text{free}}$ occurs at around $C_g = C_{sa}$.

Accepting that $r_{2\text{bound}} > r_{2\text{free}}$, it follows from Eq. [2] and Eq. [5] that, in all cases:

$$\Delta R_2 < r_{2\text{bound}} \cdot C_g \qquad [15]$$

It should be noted that experimental imprecision in R_2 measurement (and R_1 measurement, as C_g is calculated using Eq. [8]) may violate this inequality, and may lead to calculated values of $C_{sa} \leq 0$ mM. For transverse relaxivity, $r_{2\text{bound}}$ is much higher than $r_{2\text{free}}$ at all B_0 values; for longitudinal relaxivity, $r_{1\text{bound}}$ is much higher than $r1_{\text{free}}$ at low B_0 but both are effectively equivalent at very
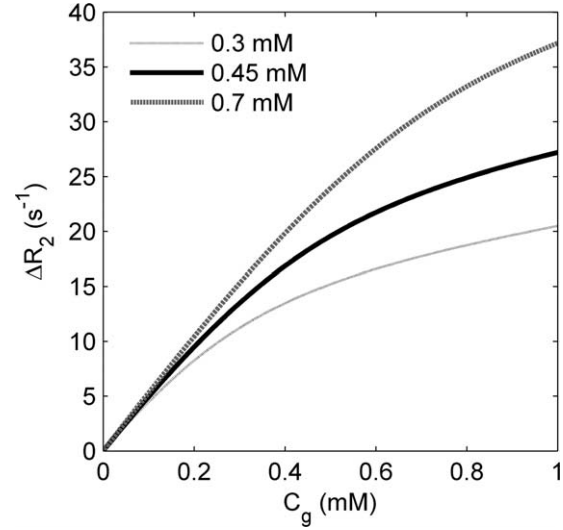

FIG. 1. Modeled variation of ΔR_2 with gadofosveset concentration for three serum albumin concentrations, based on Eq. [14], assuming values of $K_a = 11.0$ mM^{-1}, $r_{2\text{bound}} = 60.0$ s^{-1} mM^{-1}, $r_{2\text{free}} = 6.1$ s^{-1} mM^{-1} (29)

high B_0 (34). This variation with field strength means that at low B_0 any imprecision in R_2 measurement has a much greater influence on calculated C_g (Eq. [8]), therefore, it is expected that the model may not be applicable at low B_0 values.

METHODS

In Vitro Validation

Model validation was carried out by calculating C_{sa} (using Eq. [13]) for a range of in vitro solutions. This requires values of K_a, ΔR_1, ΔR_2, $r_{2\text{bound}}$, $r_{2\text{free}}$, $r_{1\text{bound}}$, and $r_{1\text{free}}$. ΔR_1 and ΔR_2 were measured within the study, a fixed K_a value of 11.0 mM^{-1} was assumed in calculations (27,28,32), and relaxivity values were derived from the data presented in this study (as values for matching experimental conditions could not be found in the literature).

In vitro solutions of gadofosveset (Vasovist) were prepared for use at 3.0T with phosphate-buffered saline (PBS, dry powder reconstituted with deionized water, pH 7.4, Sigma Aldrich, St Louis, MO) and human serum albumin (HSA, Cohn fraction V lyophilized powder, Sigma Aldrich, in PBS). Solutions were created at C_{sa} and C_g concentrations between 0 and 1.0 mM; a total of 26 combinations of gadofosveset and HSA were prepared. A set of solutions containing the nonbinding contrast agent gadopentetate dimeglumine (Magnevist, Bayer Healthcare Pharmaceuticals, Germany) in HSA at $C_{sa} = 0.7$ mM were created to act as a control. The solutions measured at 4.7T used bovine serum albumin (BSA, Cohn fraction V lyophilized powder, Sigma Aldrich, in PBS) in place of HSA, within the same range of concentrations.

$r_{1\text{free}}$ and $r_{2\text{free}}$ were calculated by applying the linear model in Eq. [1] to the ΔR_1 and ΔR_2 values for the gadofosveset–PBS samples ($C_{sa} = 0$ mM), where no binding was assumed. To prevent the relaxation rates for any given

gadofosveset–albumin sample($C_{sa} > 0$ mM) influencing the relaxivity values subsequently used to calculate C_{sa} for that sample, bound relaxivity was calculated by setting aside one sample and applying a one-parameter model fit to the remaining subset of ΔR_1 and ΔR_2 values (using Eq. [14]). This process was repeated for each sample until a set of individual r_{1bound} and r_{2bound} values was created. The calculated relaxivities associated with each excluded sample (and its measured ΔR_1 and ΔR_2 values) were used in the subsequent C_{sa} calculation for that sample using Eq. [13].

In Vitro Data Acquisition: 3.0T

Tubes were placed vertically within a cardiac coil in a 3.0T Philips Achieva TX system. Solutions were maintained at a temperature of 34–37°C with warm air flow, verified with a fiber optic temperature probe in an adjacent water tube. T_1 values were measured using a spin echo inversion recovery sequence with 5 inversion times (TI = 50, 225, 371, 1665, 4875 ms), repetition time (TR) = 5000 ms, echo time (TE) = 6.2 ms. T_2 values were measured using a multi-echo sequence with eight echo times (TE = 50, 100, 150, 200, 250, 300, 350, 400 ms), TR = 1000 ms. Additional parameters common to both T_1 and T_2 measurement: field of view = 231 × 231 mm; matrix size = 240 × 240 pixels; single coronal (horizontal) slice; slice thickness = 10 mm.

In Vitro Data Acquisition: 4.7T

Tubes were placed vertically in a cylindrical cradle of diameter 60 mm and inserted into a 63-mm quad coil in a horizontal bore 4.7T magnet with Bruker console running ParaVision 5.1 software (Bruker BioSpin MRI GmbH, Ettlingen, Germany). Solutions were maintained at a temperature of 37°C with warm air flow, verified with a fiber optic temperature probe in an adjacent water tube. R_1 values were measured using a RARE saturation recovery imaging sequence (35), with nine recovery times (57.2, 68.5, 78.5, 88.5, 103.5, 183.5, 283.5, 383.5, 983.5 ms) and a TE of 11 ms. R_2 values were measured using a multi-slice multi-echo (MSME) sequence, with 20 equally spaced TE values from 11 to 220 ms and a TR of 1000 ms. Additional parameters common to both T_1 and T_2 measurement: field of view = 60 × 60 mm; matrix size = 256 × 256 pixels; RARE factor = 2; averages = 1; centric encoding; single coronal (horizontal) slice; slice thickness = 1 mm.

Relaxation Rates

A circular region of interest (ROI) was drawn within each tube and the mean signal intensity (SI) of each ROI measured using ImageJ software (v1.42q, Rasband, W.S., ImageJ, U. S. National Institutes of Health, Bethesda, MD, http://imagej.nih.gov/ij/, 1997–2011). SI values at 4.7T were adjusted for noise bias using a simple Rician correction (36), based on mean standard deviations of four background regions in each image. R_1 values at 4.7T and R_2 values at 3.0T and 4.7T, along with 95% confidence intervals, were determined from two-parameter nonlinear fits to Eqs. [16] and [17], respectively, using

MATLAB (v 7.9, MathWorks, Natick, MA). R_1 calculation at 3.0T included an extra term for TR (Eq. 18).

$$SI = S_0.\left(1 - e^{-TI.R1}\right) \qquad [16]$$

$$SI = S_0.e^{-TE.R2} \qquad [17]$$

$$SI = S_0.\left(1 - b.e^{-TI.R1} + e^{-TR.R1}\right) \qquad [18]$$

where S_0 represents the fully recovered SI value and b is a factor accounting for imprecision in the 180° inversion pulse, applied to each ROI.

Contrast agent-induced changes in relaxation rate ($\Delta R_{1,2}$) were calculated by subtracting $R_{1,2}$ values for each non-Gd C_{sa} solution ($C_g = 0$) from equivalent Gd-containing C_{sa} solutions ($C_g > 0$).

In Vivo Feasibility Assessment: 3.0T

A total of seven healthy volunteers (five male, mean age 36 ± 10 years, mean weight 81 ± 15 kg) underwent pre- and postcontrast short-axis cardiac scans on a 3.0T Siemens Skyra system at Northwestern Memorial Hospital, Chicago. The study was approved by the Institutional Review Board (IRB) at Northwestern University, with informed consent obtained from all participants. IRB approval did not include provision for taking blood samples, therefore per-volunteer measures of hematocrit and blood albumin were not available.

Images were acquired as part of a larger study mapping flow patterns in thoracic aortic aneurisms (TAA) in different progression stages. Myocardial T_1 and T_2 values with administration of an MR contrast agent were also acquired to study changes of these parameters associated with inflammatory and connective tissue diseases that are in turn associated with the progression of TAA. A small timing bolus of 1.0–2.0 ml of gadofosveset (Ablavar) was used to establish arrival time and was followed by a main bolus of 6.2–8.8 mL, giving a total dose of 0.12 mL/kg (0.03 mmol/kg). A modified Look-Locker inversion recovery (MOLLI) sequence (37) with motion correction (38) (field of view = 270 × 360 mm, matrix size = 144 × 256 pixels, flip angle = 35°, TR = 313.45 ms, TE = 1.13 ms, bandwidth/pixel = 975 Hz) was used for T_1, with T_1 maps created inline by the system software. This version of the MOLLI sequence consisted of two inversions, with three images acquired after the first inversion (initial effective TI of 120 ms, and RR interval added to the other two acquisitions), and five images acquired after the second inversion (first effective TI of 200 ms; 200 ms + RR for subsequent acquisitions). Images were acquired with a specific trigger delay to select for end diastole. MOLLI acquisition was followed by a T_2 mapping sequence using a single-shot T_2-prepared steady-state free precession (SSFP) acquisition with three T_2-preparation echo times: 0, 24, and 55 ms (39) (field of view = 337 × 450 mm, matrix size = 144 × 192 pixels, TR = 201.88 ms, TE = 1.07 ms, flip angle = 40°, bandwidth/pixel = 930 Hz). For all sequences, 8 mm slices were acquired at cardiac short axis base, mid and apex locations. Postcontrast images were acquired at up to three time points for each volunteer,

Table 1
Main Bolus and Image Acquisition Times for Volunteers[a]

Volunteer no.	Main bolus	Measurement					
		T_1 [1]	T_2 [1]	T_1 [2]	T_2 [2]	T_1 [3]	T_2 [3]
1	07:08	14:31	16:47	–	–	–	–
2	03:52	08:57	11:19	38:34	39:35	54:06	55:53
3	02:35	07:10	08:10	29:12	30:15	–	–
4	04:15	29:17	31:44	–	–	–	–
5	08:24	41:43	43:25	–	–	–	–
6	03:24	23:45	25:02	28:09	29:29	39:23	40:38
7	03:06	05:34	07:21	18:34	20:16	27:02	28:36

[a]Time from first administration of contrast agent (timing bolus), MM:SS.

with T_2 image acquisition occurring 1–2 min after T_1 acquisition (Table 1). The mid-point between T_1 and T_2 image acquisitions was used as the postcontrast reference time for each data point when plotting the results.

ROIs were drawn within the left ventricle and within the myocardium on each pre- and postcontrast T_1 and T_2 map at the middle of the short axis view, and median and standard deviation values derived using MATLAB. For albumin calculation, each ROI is considered as a single well-mixed compartment, which is a valid assumption for the left ventricle, where gadofosveset is entirely intravascular, but is a simplification of conditions in the myocardium, where ΔR_1 and ΔR_2 are influenced by gadofosveset in vascular and extravascular spaces.

As the described T_2 acquisition protocol is optimized for myocardial T_2 measurement it is likely to underestimate the longer T_2 of native blood, which may lead to an underestimation in ΔR_2 calculation. To investigate this influence, an underestimation in ΔR_2 was simulated and the effect on calculated albumin values observed. Expected ΔR_2 values were obtained using Eq. [14] across a range of C_{sa} and C_g values, based on derived in vitro 3.0T relaxivities; these ΔR_2 values were then reduced by an arbitrary 10% and C_{sa} values calculated according to Eq. [13].

RESULTS

In Vitro Data at 3.0T and 4.7T

Mean individual gadofosveset relaxivity values measured at 3.0T and 4.7T for the range of C_{sa}–C_g combinations are given in Table 2; standard deviations indicate the variance in calculated relaxivity.

Figure 2 shows model fits (Eq. [14]) plotted against actual ΔR_1 and ΔR_2 gadofosveset data points at 3.0T and 4.7T, using the mean individual relaxivities in Table 2. A linear fit to the gadopentetate data is also shown.

In Figure 3 calculated C_{sa} values (using Eq. [13]) are compared with actual values for each solution using individually derived relaxivity values at 3.0T and 4.7T. Four data points violated the inequality described in Eq. [15], and were therefore excluded from the 4.7T calculations. The model-derived C_{sa} values correlate with actual C_{sa} at a statistically significant level at both field strengths (Pearson correlation coefficients of 0.85 and 0.88 for 3.0T and 4.7T, respectively).

Volunteer Data at 3.0T

Precontrast T_1 values in the left ventricle and myocardium were in the range 1493–1818 ms and 1099–1124 ms, respectively. Precontrast T_2 values in the left ventricle and myocardium were in the range 117–158 ms and 43–47 ms, respectively. Calculated gadofosveset and albumin concentrations in the left ventricle and myocardium are shown in Figure 4, with data for all seven volunteers plotted against time from first bolus administration. The models for calculating gadofosveset (Eq. [8]) and albumin (Eq. [13]) concentrations used the 3.0T (PBS/HSA) relaxivity values shown in Table 2.

The effect of an underestimation in ΔR_2 on calculated C_{sa} was simulated at a range of C_g values, using the 3.0T relaxivity values from Table 2. Simulations showed that a 10% underestimation in ΔR_2 led to an underestimation in calculated C_{sa}. This model underestimation increases as actual C_{sa} increases, and is more pronounced at lower C_g. For example, at $C_{sa} = 1.0$ mM calculated C_{sa} is 0.6 mM lower than actual C_{sa} for $C_g = 0.1$ mM, but calculated C_{sa} is only 0.2 mM lower than actual C_{sa} for $C_g = 1.0$ mM.

DISCUSSION

Increased capillary leakage is symptomatic of a range of pathologies and healthy processes, resulting in rapid wash-in and wash-out of small molecule contrast agents and an increased transfer of macromolecules, including intravascular albumin, to the interstitial space. In vivo measurement of extravascular albumin content is not straightforward, although a range of invasive techniques are currently available. This study has explored the possibility of utilizing the albumin-binding properties of the

Table 2
Mean Individual Gadofosveset Relaxivity Values (and SDs)

Relaxivity (s^{-1} mM^{-1})	3.0T		4.7T	
	This study (PBS/HSA)	Literature[a]	This study (PBS/BSA)	Literature[a]
r_{1bound}	10.0 (0.1)	9.9	6.5 (0.0)	6.9
r_{1free}	6.1 (0.3)	5.3	4.5 (0.1)	5.5
r_{2bound}	100.9 (0.7)	60.0	60.0 (0.2)	60.0
r_{2free}	7.5 (0.2)	6.1	10.7 (0.2)	6.9

[a]Literature values from (29), where $r_{1,2free}$ are measured in water at 37°C and $r_{1,2bound}$ are observed relaxivities in bovine plasma at 37°C.
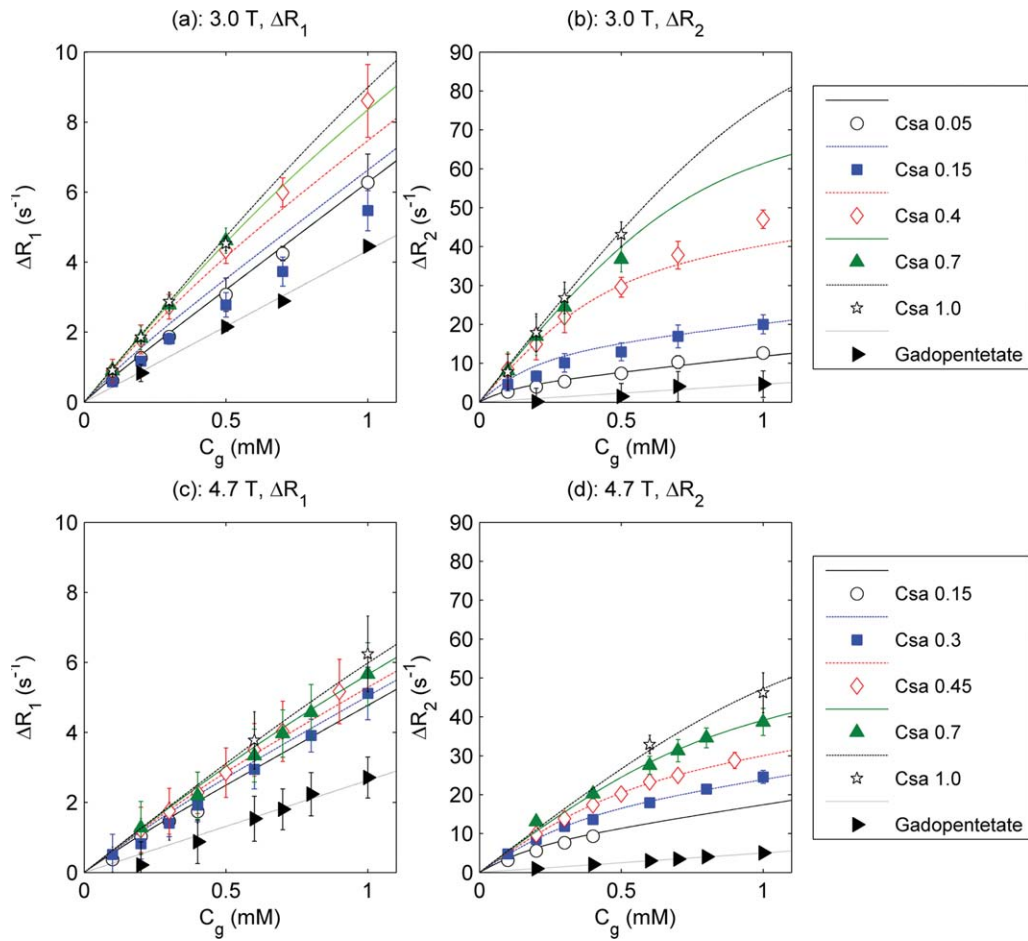
FIG. 2. ΔR_1 (left column) and ΔR_2 (right column) values for gadofosveset at a range of albumin concentrations and for gadopentetate at 0.7 mM, at 3.0T (upper row) and 4.7T (lower row). Points represent measured values (with 95% confidence intervals); gadofosveset lines represent model fit based on relaxivities in Table 2; gadopentetate lines represent linear fit.

Gd-based contrast agent gadofosveset to generate a novel and location-specific noninvasive method for measuring levels of albumin at moderate to high magnetic field strengths. Pre- and postcontrast R_1 and R_2 measurements are regularly carried out in MRI; the models presented here combine these changes in relaxation rate with
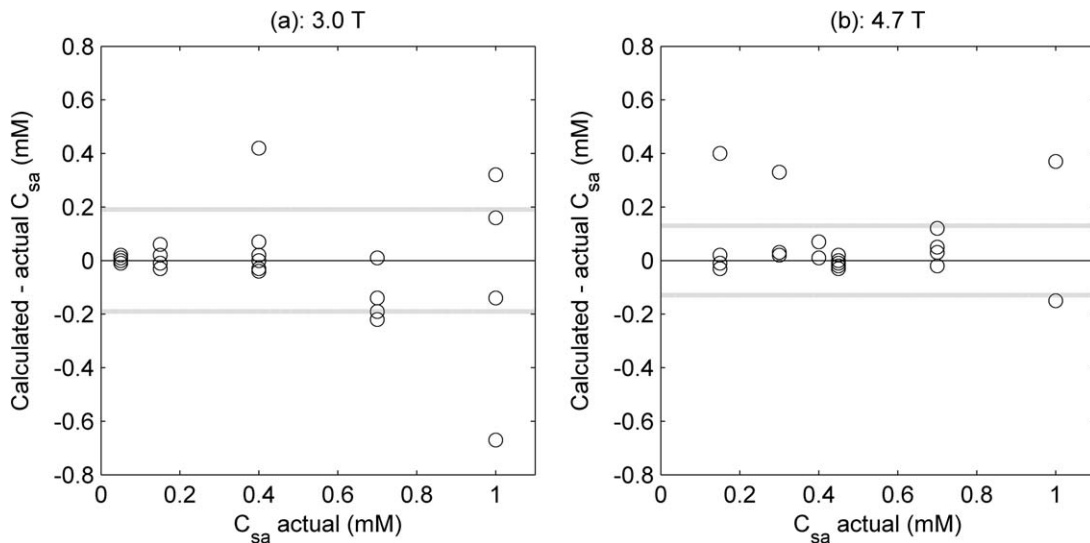

FIG. 3. Bland–Altman plots of actual versus difference (calculated – actual) C_{sa} at 3.0T (26 plotted points) (**a**) and 4.7T (24 plotted points) (**b**). Dashed lines indicate standard deviation of difference
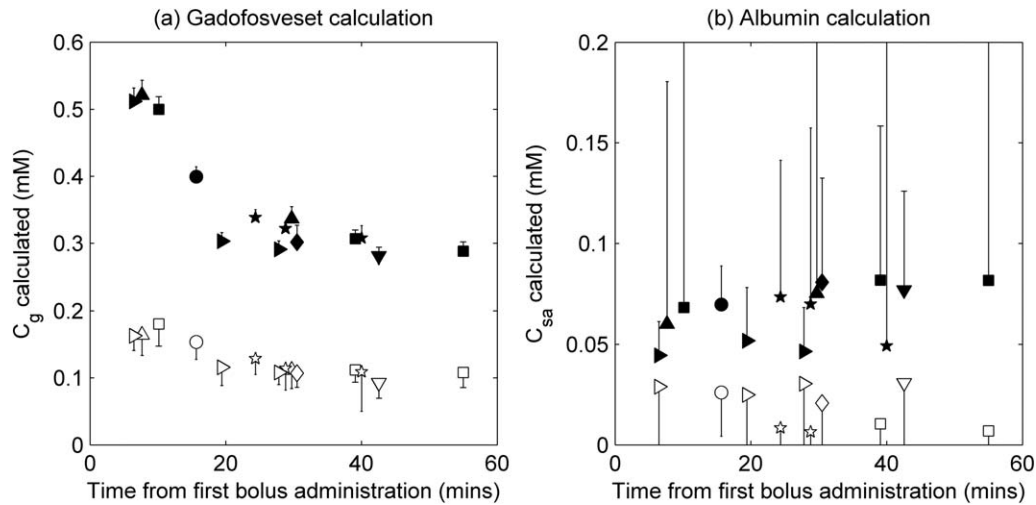
FIG. 4. Calculated gadofosveset (**a**) and albumin (**b**) concentrations in myocardium (open symbols) and left ventricle (filled symbols) in healthy volunteers at 3.0T. Each symbol shape represents a different volunteer; values are plotted against time from first administration of contrast agent (to mid-point between T_1 and T_2 image acquisition times); error bars indicate uncertainty in calculations, calculated by propagation of errors using standard deviation of initial R_1 and R_2 ROI measurements (errors are symmetrical about data point, but only one side shown to aid clarity)

calculated relaxivity values and a literature binding affinity value to produce a basic measure of tissue albumin concentration.

In Vitro Model Validation

Calculated r_1 and r_2 relaxivity values at both 3.0T and 4.7T are in general agreement with previously published values (Table 2), although it is difficult to find directly equivalent experimental conditions for comparison. Using mean calculated relaxivity values, the model represents a good fit to gadofosveset ΔR_1 and ΔR_2 data points at low and high C_{sa} values (Fig. 2), suggesting that the assumption of a single binding site on the albumin molecule is adequate at these concentration levels. The primary binding site is known to provide the greatest contribution to relaxivity (28), and it is unlikely that C_g levels would be sufficiently high in vivo during the post-bolus phase to necessitate inclusion of additional binding sites in this model (32). An attempt to model the data with second and third binding sites filled sequentially according to relative C_g and C_{sa} concentrations, using binding affinity values of 0.84 and 0.26 mM^{-1} (28), did not noticeably alter the model fits to measured data points (data not shown).

Excluding negative calculated C_{sa} values resulting from measurement imprecision and comparing the remaining calculated and actual C_{sa} values (Fig. 3), the model-derived C_{sa} values correlate with actual C_{sa} at a statistically significant level at both 3.0T and 4.7T.

The albumin-calculation model presented here is expected to work well at higher B_0 field strengths (3.0T and above), where there is a large difference between r_{2bound} and r_{2free} but a small difference between r_{1bound} and r_{1free}. At low fields, r_{1bound} is close to r_{2bound} and the difference between ΔR_1 and ΔR_2 is small. In this case, the precision of the model input parameters would be insufficient to overcome the sensitivity of the model to

the variability in those parameters, leading to a breakdown of the model. At very high B_0 field strengths, r_{1bound} and r_{1free} values for gadofosveset may be considered equivalent and the model may be simplified to incorporate a linear relationship between ΔR_1 and C_g. The C_g calculation described in Eq. [8] may then be represented as $C_g = \Delta R_1 / r_1$.

An underlying correlation between relaxivity and protein content has been shown in previous studies for Gd-based contrast agents not conventionally described as albumin binding (40,41). In vitro gadopentetate ΔR_2 data points are well represented here by a linear fit (Fig. 2), suggesting no observable influence of weak binding on contrast agent relaxivity at the albumin levels used in this study. Without separate bound and free transverse relaxivities, gadopentetate provides no means of estimating C_{sa} through application of the model presented here. The high binding affinity of gadofosveset makes it a much more sensitive biomarker of albumin.

In Vivo Feasibility

Gadofosveset-enhanced cardiovascular imaging is an area of active research (42–46), and likely to remain so in North America where the agent is available under the trade name Ablavar. One potential clinical application of the technique for calculating albumin concentration relates to myocardial infarction, therefore a feasibility assessment using human cardiac images was considered relevant. Cardiac imaging has the advantage of enabling direct comparison of calculated albumin values from blood in the left ventricle and from highly perfused myocardial tissue. However, before the model can be assessed, motion correction and other technical challenges must be overcome.

Precontrast T_1 and T_2 values generally correlate well with literature values (47–49), although longer T_2 values in blood have been quoted elsewhere (50). Combining

data from seven volunteers with images acquired at a range of time points gave remarkably consistent values of the two model input variables ΔR_1 and ΔR_2, and supported calculation of appropriate C_g values in both the left ventricle and the myocardium (Fig. 4a). As expected, gadofosveset concentration peaks at the earliest time points postbolus and decreases toward an equilibrium value, although this was not a dynamic acquisition therefore the temporal resolution is such that the bolus peak is not fully described.

At a dose of 0.03 mmol per kg, the average blood concentration of gadofosveset for an 81 kg adult with a total blood volume of 6.4 L would be 0.4 mM; allowing for some extravasation and excretion, the gadofosveset values calculated here in the left ventricle appear reasonable. For a small molecule agent such as gadopentetate, approximately 50% may diffuse to the extravascular space from the blood on the first pass through the capillary bed (51). Although, as a "blood pool" agent, gadofosveset may be expected to remain predominantly within the intravascular space, at high concentrations (immediately after bolus injection, for example) the bound fraction will be low and the extravasation rate may be similar to that of a conventional agent (52). A study in rabbits showed that 61% of injected gadofosveset was still in the blood at 1 min postinjection (32). Certainly, a reduction in C_g between the left ventricle and myocardium is expected, as noted in the relative values here.

Unlike gadofosveset, albumin concentration is expected to remain consistent within an individual for the image acquisition duration. Although there is some within-subject variability (Fig. 4b), this is a representation of the imprecision in data acquisition and does not correlate with time postbolus. The mean calculated albumin concentration in the left ventricle of the seven volunteers was 0.07 mM (range, 0.04–0.08 mM); in the myocardium the mean calculated C_{sa} was 0.02 mM (range, 0.01–0.03 mM).

A reference measure of albumin concentration was not available for comparison. Serum albumin levels in plasma (C_{sa_plasma}) are expected to be approximately 3.5–5.0 g/dL (0.52–0.74 mM) (53). Assuming a hematocrit (Hct) of 0.42, this equates to albumin levels in whole blood of 0.30–0.43 mM (where blood concentration $= C_{sa\_plasma}\ (1 - \text{Hct})$). Previous studies quote interstitial fluid albumin concentrations ($C_{sa\_interstitial}$) of 0.2–0.4 mM (10,11,54). However, the myocardium ROI contains intravascular, extravascular extracellular and intracellular spaces. Neglecting the intracellular space, as gadofosveset cannot directly access it, and assuming an extracellular volume fraction (EVF) of 0.25 (55), a myocardial blood volume (MBV) of 8% (56) and a hematocrit in capillaries (Hct_{cap}) of 0.25, tissue albumin (C_{sa_tissue}, measurable using gadofosveset) may be expected to be in the range 0.07–0.11 mM (where $C_{sa\_tissue} = \text{MBV}.$ $(C_{sa\_plasma}.(1 - \text{Hct}_{cap})) + C_{sa\_interstitial}.$ $(\text{EVF} - \text{MBV})$). This range of expected values assumes that all blood vessels in the myocardium are capillaries; in reality, a proportion would be larger than capillaries and would, therefore, have a higher Hct, leading to a slightly lower range of expected C_{sa_tissue} values.

Calculated C_{sa} values were lower than might be expected in healthy volunteers. Factors contributing to

an underestimation could include the relative timings of the T_1 and T_2 measurements, the separation of gadofosveset delivery into a timing bolus and a main bolus, and the potential incompatibility of translated in vitro relaxivities (for example, due to fundamental differences between in vitro and in vivo measurement of relaxivity (57), although the inclusion of albumin in the in vitro samples used for relaxivity calculation will moderate this issue). The selected scanning parameters were optimized for myocardial tissue and are likely to lead to an underestimation in ΔR_2 in the left ventricle. The large error bars on the C_{sa} calculations in the left ventricle (Fig. 4b) confirm the difficulty in applying the model to left ventricular data acquired under conditions optimized for myocardial measurement. Simulated data suggest that underestimation in ΔR_2 may result in a substantial underestimation in calculated C_{sa}. However, it should be noted that the described method may not be appropriate or necessary in the left ventricle as albumin levels in blood can be readily measured from blood samples. The primary utility of the method may be in providing measurement of albumin concentration in tissue, where C_g is lower and C_{sa} is conventionally difficult to acquire.

A previous study using the contrast agent gadobenate (58), which has a much lower albumin binding affinity than gadofosveset (59), suggested that renal protein leakage could be identified by analyzing tubular flow differences following injection of two contrast agents, one binding and one nonbinding. Attempts have also been made to map protein levels by utilizing the distinct field dependency of the bound and free gadofosveset molecule (termed delta relaxation enhanced MR, DREMR) (60,61), although this approach requires the use of additional hardware to modulate B_0 field strength. The advantage of the method described in this study over either of these approaches is that it only requires a single contrast agent injection and may be readily derived from routinely acquired R_1 and R_2 measurements using conventional equipment.

CONCLUSIONS

The model presented here demonstrates the feasibility of determining in vitro serum albumin concentration using pre- and postgadofosveset measurements of R_1 and R_2 at high B_0 fields. The method was successfully validated using in vitro samples at 3.0T and 4.7T. Feasibility assessment in a small number of human volunteers was performed using cardiac images, and consistent ΔR_1, ΔR_2 and C_g values were determined. Underestimation of C_{sa} may be the result of several contributing factors, including the timing of the image acquisitions and translation of in vitro relaxivities. A more effective application of this method may be in tumor angiogenesis, where increased extravascular macromolecular leakage rates are observed and imaging is less restricted by cardiac or respiratory motion. Further in vivo assessment is suggested, to include: simultaneous T_1 and T_2 measurement; additionally acquiring images between the timing bolus and the main bolus; and blood sampling to establish hematocrit and reference blood albumin levels.

This novel approach may enable noninvasive assessment of extravascular leakage of albumin, utilizing parameters acquired during routine imaging, in regions where implementation of invasive techniques for measurement of interstitial albumin is conventionally challenging. A range of potential clinical applications are envisaged, including assessment of myocardial infarction, tumor angiogenesis, and response to treatment.

ACKNOWLEDGMENTS

REFERENCES

1. Doweiko JP, Nompleggi DJ. Role of albumin in human physiology and pathophysiology. J Parenter Enteral Nutr 1991;15:207–211.
2. Bhattacharya AA, Grune T, Curry S. Crystallographic analysis reveals common modes of binding of medium and long-chain fatty acids to human serum albumin. J Mol Biol 2000;303:721–732.
3. Kratochwil NA, Huber W, Muller F, Kansy M, Gerber PR. Predicting plasma protein binding of drugs: a new approach. Biochem Pharmacol 2002;64:1355–1374.
4. Nicholson JP, Wolmarans MR, Park GR. The role of albumin in critical illness. Br J Anaesth 2000;85:599–610.
5. Bradley J, Cunningham K, Jackson V. Serum protein levels in critically ill surgical patients. Intensive Care 1981;7:291–295.
6. Djousse L, Rothman KJ, Cupples LA, Levy D, Ellison RC. Serum albumin and risk of myocardial infarction and all-cause mortality in the Framingham offspring study. Circulation 2002;106:2919–2924.
7. Ballmer PE. Causes and mechanisms of hypoalbuminaemia. Clin Nutr 2001;20:271–273.
8. Saeed M, Van Dijke CF, Mann JS, Wendland MF, Rosenau W, Higgins CB, Brasch RC. Histologic confirmation of microvascular hyperpermeability to macromolecular MR contrast medium in reperfused myocardial infarction. J Magn Reson Imaging 1998;8:561–567.
9. Seitz RJ, Wechsler W. Immunohistochemical demonstration of serum proteins in human cerebral gliomas. Acta Neuropathol 1987;73:145–152.
10. Poulsen HL. Subcutaneous interstitial fluid albumin concentration in long-term diabetes-mellitus. Scand J Clin Lab Invest 1973;32:167–173.
11. Haaverstad R, Romslo I, Larsen S. Protein concentration of subcutaneous interstitial fluid in the human leg. J Vasc Res 1996;16:111–117.
12. Ellmerer M, Schaupp L, Brunner GA, Sendlhofer G, Wutte A, Wach P, Pieber TR. Measurement of interstitial albumin in human skeletal muscle and adipose tissue by open-flow microperfusion. Am J Physiol Endocrinol Metab 2000;278:E352–E356.
13. Waterton JC. Translational magnetic resonance imaging and spectroscopy: opportunities and challenges. In: Garrido L, Beckmann N, editors. New applications of NMR in drug discovery and development. Cambridge, UK: RSC press; 2013. p 333–360.
14. Daldrup H, Shames DM, Wendland M, Okuhata Y, Link TM, Rosenau W, Lu Y, Brasch RC. Correlation of dynamic contrast-enhanced MR imaging with histologic tumor grade: comparison of macromolecular and small-molecular contrast media. AJR Am J Roentgenol 1998;171:941–949.
15. Roberts TPL, Turetschek K, Preda A, Novikov V, Moeglich M, Shames DM, Brasch RC, Weinmann HJ. Tumor microvascular changes to anti-angiogenic treatment assessed by MR contrast media of different molecular weights. Acad Radiol 2002;9(Suppl. 2):S511–S513.
16. Schwitter J, Saeed M, Wendland MF, Derugin N, Canet E, Brasch RC, Higgins CB. Influence of severity of myocardial injury on distribution of macromolecules: extravascular versus intravascular gadolinium-based magnetic resonance contrast agents. J Am Coll Cardiol 1997;30:1086–1094.
17. Aime S, Caravan P. Biodistribution of gadolinium-based contrast agents, including gadolinium deposition. J Magn Reson Imaging 2009;30:1259–1267.
18. Lauffer RB, Parmelee DJ, Dunham SU, Ouellet HS, Dolan RP, Witte S, McMurry TJ, Walovitch RC. MS-325: albumin-targeted contrast agent for MR angiography. Radiology 1998;207:529–538.
19. Barrett T, Kobayashi H, Brechbiel M, Choyke PL. Macromolecular MRI contrast agents for imaging tumor angiogenesis. Eur J Radiol 2006;60:353–366.
20. Bremerich J, Bilecen D, Reimer P. MR angiography with blood pool contrast agents. Eur Radiol 2007;17:3017–3024.
21. Puig J, Blasco G, Essig M, et al. Albumin-binding MR blood pool contrast agent improves diagnostic performance in human brain tumour: comparison of two contrast agents for glioblastoma. Eur Radiol 2012:1–9.
22. Milot L, Haider M, Foster L, McGregor C, Law C. Gadofosveset trisodium in the investigation of focal liver lesions in noncirrhotic liver: early experience. J Magn Reson Imaging 2012;36:738–742.
23. Thouet T, Schnackenburg B, Kokocinski T, Fleck E, Nagel E, Kelle S. Visualization of chronic myocardial infarction using the intravascular contrast agent MS-325 (Gadofosveset) in patients. Sci World J 2012:1–6.
24. Phinikaridou A, Andia ME, Protti A, Indermuchle A, Shah A, Smith A, Warley A, Botnar RM. Noninvasive magnetic resonance imaging evaluation of endothelial permeability in murine atherosclerosis using an albumin-binding contrast agent. Circulation 2012;126:707–719.
25. Leporq B, Dumortier J, Pilleul F, Beuf O. 3D-liver perfusion MRI with the MS-325 blood pool agent: A noninvasive protocol to asses liver fibrosis. J Magn Reson Imaging 2012;35:1380–1387.
26. Richardson OC, Scott MLJ, Tanner SF, Waterton JC, Buckley DL. Overcoming the low relaxivity of gadofosveset at high field with spin locking. Magn Reson Med 2012;68:1234–1238.
27. Eldredge HB, Spiller M, Chasse JM, Greenwood MT, Caravan P. Species dependence on plasma protein binding and relaxivity of the gadolinium-based MRI contrast agent MS-325. Invest Radiol 2006;41:229–243.
28. Caravan P, Cloutier NJ, Greenfield MT, et al. The interaction of MS-325 with human serum albumin and its effect on proton relaxation rates. J Am Chem Soc 2002;124:3152–3162.
29. Rohrer M, Bauer H, Mintorovitch J, Requardt M, Weinmann H-J. Comparison of magnetic properties of MRI contrast media solutions at different magnetic field strengths. Invest Radiol 2005;40:715–724.
30. Muller RN, Raduchel B, Laurent S, Platzek J, Pierart C, Mareski P, Vander Elst L. Physicochemical characterization of MS-325, a new gadolinium complex, by multinuclear relaxometry. Eur J Inorg Chem 1999;1999:1949–1955.
31. Aime S, Fasano M, Terreno E, Botta M. Protein-bound metal chelates. In: Merbach AE, Toth E, editors. The chemistry of contrast agents in medical magnetic resonance imaging. Chichester: John Wiley & Sons; 2001. p 193–242.
32. Port M, Corot C, Violas X, Robert P, Raynal I, Gagneur G. How to compare the efficiency of albumin-bound and nonalbumin-bound contrast agents in vivo. Invest Radiol 2005;40:565–573.
33. Aime S, Chiaussa M, Digilio G, Gianolio E, Terreno E. Contrast agents for magnetic resonance angiographic applications: 1H and 17O NMR relaxometric investigations on two gadolinium(III) DTPA-like chelates endowed with high binding affinity to human serum albumin. J Biol Inorg Chem 1999;4:766–774.
34. Caravan P, Farrar CT, Frullano L, Uppal R. Influence of molecular parameters and increasing magnetic field strength on relaxivity of gadolinium- and manganese-based T1 contrast agents. Contrast Media Mol Imaging 2009;4:89–100.
35. Hennig J, Nauerth A, Friedburg H. RARE imaging: a fast imaging method for clinical MR. Magn Reson Med 1986;3:823–833.

36. Henkelman RM. Measurement of signal intensities in the presence of noise in MR images. Med Phys 1985;12:232–233.

37. Messroghli DR, Radjenovic A, Kozerke S, Higgins DM, Sivananthan MU, Ridgway JP. Modified Look-Locker inversion recovery (MOLLI) for high-resolution T1 mapping of the heart. Magn Reson Med 2004; 52:141–146.

38. Xue H, Shah S, Greiser A, Guetter C, Littmann A, Jolly M-P, Arai AE, Zuehlsdorff S, Guehring J, Kellman P. Motion correction for myocardial T1 mapping using image registration with synthetic image estimation. Magn Reson Med 2012;67:1644–1655.

39. Giri S, Chung YC, Merchant A, Mihai G, Rajagopalan S, Raman SV, Simonetti OP. T2 quantification for improved detection of myocardial edema. J Cardiovasc Magn Reson 2009;11:56.

40. Wang Y, Spiller M, Caravan P. Evidence for weak protein binding of commercial extracellular gadolinium contrast agents. Magn Reson Med 2010;63:609–616.

41. Bagher-Ebadian H, Paudyal R, Nagaraja TN, Croxen RL, Fenstermacher JD, Ewing JR. MRI estimation of gadolinium and albumin effects on water proton. Neuroimage 2011;54(Suppl. 1):S176–S179.

42. Pedersen SF, Thrysoe SA, Paaske WP, Thim T, Falk E, Ringgaard S, Kim WY. CMR Assessment of endothelial damage and angiogenesis in porcine coronary arteries using gadofosveset. J Cardiovasc Magn Reson 2011;13:10.

43. Biris O, Benefield B, Harris KR, Lee DC. A steady-state method for computation of myocardial blood volume with the intravascular contrast agent Ablavar. J Cardiovasc Magn Reson 2012;14(Suppl. 1):P49.

44. Makowski MR, Wiethoff AJ, Uribe S, et al. Congenital heart disease: Cardiovascular MR imaging by using an intravascular blood pool contrast agent. Radiology 2011;260:680–688.

45. Ritter CO, Wilke A, Wichmann T, Beer M, Hahn D, Kostler H. Comparison of intravascular and extracellular contrast media for absolute quantification of myocardial rest-perfusion using high-resolution MRI. J Magn Reson Imaging 2011;33:1047–1051.

46. Wagner M, Rosler R, Lembcke A, et al. Whole-heart coronary magnetic resonance angiography at 1.5 tesla: Does a blood-pool contrast agent improve diagnostic accuracy? Invest Radiol 2011;46:152–159.

47. Noeske R, Seifert F, Rhein KH, Rinneberg H. Human cardiac imaging at 3 T using phased array coils. Magn Reson Med 2000;44:978–982.

48. Zhao J, Clingman C, Narvainen M, Kauppinen R, van Zijl P. Oxygenation and hematocrit dependence of transverse relaxation rates of blood at 3T. Magn Reson Med 2007;58:592–597.

49. Zaman A, Higgins DM, Kouwenhoven M, Kidambi A, Greenwood JP, Plein S. Robust myocardial T2 and T2* mapping at 3T. J Cardiovasc Magn Reson 2012;14:(Suppl. 1):P306.

50. Stanisz GJ, Odrobina EE, Pun J, Escaravage M, Graham SJ, Bronskill MJ, Henkelman RM. T1, T2 relaxation and magnetization transfer in tissue at 3T. Magn Reson Med 2005;54:507–512.

51. Brasch RC. Rationale and applications for macromolecular Gd-based contrast agents. Magn Reson Med 1991;22:282–287.

52. Bane O, Lee DC, Benefield B, Markl M, Carr J, Carroll TJ. A pilot study of leakage and compartmentalization of the contrast agent Ablavar. J Cardiovasc Magn Reson 2013;15(Suppl. 1):E7.

53. Rothschild M, Oratz M, Schreiber S. Albumin synthesis. N Engl J Med 1972;286:748–757.

54. Fogh-Andersen N, Altura BM, Altura BT, Siggaardandersen O. Composition of interstitial fluid. Clin Chem 1995;41:1522–1525.

55. Kellman P, Wilson JR, Xue H, Bandettini WP, Shanbhag SM, Druey KM, Ugander M, Arai AE. Extracellular volume fraction mapping in the myocardium, part 2: Initial clinical experience. J Cardiovasc Magn Reson 2012;14:64.

56. Broadbent DA, Biglands JD, Larghat A, Sourbron SP, Radjenovic A, Greenwood JP, Plein S, Buckley DL. Myocardial blood flow at rest and stress measured with dynamic contrast-enhanced MRI: Comparison of a distributed parameter model with a Fermi function model. Magn Reson Med 2013;70:1591–1597.

57. Pickup S, Wood AK, Kundel HL. Gadodiamide T1 relaxivity in brain tissue in vivo is lower than in saline. Magn Reson Med 2005;53:35–40.

58. Notohamiprodjo M, Pedersen M, Glaser C, Helck AD, Lodemann K-P, Jespersen B, Fischereder M, Reiser MF, Sourbron SP. Comparison of Gd-DTPA and Gd-BOPTA for studying renal perfusion and filtration. J Magn Reson Imaging 2011;34:595–607.

59. Henrotte V, Vander Elst L, Laurent S, Muller RN. Comprehensive investigation of the non-covalent binding of MRI contrast agents with human serum albumin. J Biol Inorg Chem 2007;12:929–937.

60. Alford JK, Rutt BK, Scholl TJ, Handler WB, Chronik BA. Delta relaxation enhanced MR: Improving activation - specificity of molecular probes through R1 dispersion imaging. Magn Reson Med 2009;61: 796–802.

61. Alford JK, Sorensen AG, Benner T, Chronik AB, Handler BW, Scholl JT, Madan G, Caravan P. Direct protein imaging of inflammation in the human hand. In Proceedings of the 19th Annual Meeting of ISMRM, Montreal, Canada, 2011. Abstract 452.